ICETI

BOOK OF PROCEEDINGS

MAY 5 2022

6TH INTERNATIONAL CONFERENCE ON ENGINEERING TECHNOLOGY AND INNOVATION

WWW.ICETI.ORG

VI INTERNATIONAL CONFERENCE ON ENGINEERING TECHNOLOGY AND INNOVATION

ISSN: 2687-2323

PROCEEDINGS OF THE
V INTERNATIONAL CONFERENCE ON ENGINEERING TECHNOLOGY AND INNOVATION (ICETI) MAY 04-08, 2022
SARAJEVO, BOSNİA AND HERZEGOVİNA

Edited by
Prof. Dr. Özer Çınar

Published, 2022

info@iceti.org
www.iceti.org

info@iceti.org

SCIENTIFIC COMMITTEE

1. Prof. Dr. Adisa Parić - University of Sarajevo - Bosnia and Herzegovina
2. Prof. Dr. Aleksandar Dimitrov - Ss. Cyril and Methodius University - Macedonia
3. Prof. Dr. Anita Grozdanov - Ss. Cyril and Methodius University - Macedonia
4. Prof. Dr. Asif Šabanović – International University of Sarajevo - Bosnia and Herzegovina
5. Prof. Dr. Christos Douligeris - University of Erlangen-Nurnberg - Germany
6. Prof. Dr. Dragutin T. Mihailović - University of Novi Sad - Serbia
7. Prof. Dr. Erkan Şahinkaya – İstanbul Medeniyet University - Turkey
8. Prof. Dr. Falko Dressler - University of Paderborn - Germany
9. Prof. Dr. Houssam Toutanji – Western Michigan University - USA
10. Prof. Dr. Ian F. Akyıldız – Georgia Institute of Technology - USA
11. Prof. Dr. İsmail Usta - Marmara University - Turkey
12. Prof. Dr. Liljana Gavrilovska - Ss Cyril and Methodius University - Macedonia
13. Prof. Dr. Lukman Thalib - Qatar University - Qatar
14. Prof. Dr. M. Asghar Fazel – University of Environment - Iran
15. Prof. Dr. Mehmet Akalin - Marmara University - Turkey
16. Prof. Dr. Mehmet Kitiş – Süleyman Demirel University - Turkey
17. Prof. Dr. Muammer Koç - Hamad bin Khalifa University - Qatar
18. Prof. Dr. Özer Çınar – Yıldız Technical University - Turkey
19. Prof. Dr. Perica Paunovik - Ss. Cyril and Methodius University - Macedonia
20. Prof. Dr. Rifat Škrijelj – University of Sarajevo - Bosnia and Herzegovina
21. Prof. Dr. Samir Đug - University of Sarajevo - Bosnia and Herzegovina
22. Prof. Dr. Tanju Karanfil – Clemson University - USA
23. Prof. Dr. Tibor Biro - National University of Public Service, Budapest - Hungary
24. Prof. Dr. Ümit Alver – Karadeniz Technical University - Turkey
25. Prof. Dr. Wolfgang Gerstacker - University of Erlangen-Nurnberg - Germany
26. Prof. Dr. Yılmaz Yıldırım - Bülent Ecevit University - Turkey
27. Prof. Dr. Yousef Haik - Hamad bin Khalifa University - Qatar
28. Assoc. Prof. Dr. Alaa Al Hawari - Qatar University - Qatar
29. Assoc. Prof. Dr. Izudin Dzafic - International University of Sarajevo - Bosnia and Herzegovina
30. Assoc. Prof. Dr. Muhamed Hadziabdic - International University of Sarajevo - Bosnia and Herzegovina
31. Assoc. Prof. Dr. Nusret Drešković - University of Sarajevo - Bosnia and Herzegovina
32. Assist. Prof. Dr. Faruk Berat Akçeşme - University of Health Sciences - Turkey
33. Assist. Prof. Dr. Fouzi Tabet - German Biomass Research Center - Germany
34. Assist. Prof. Dr. Haris Gavranovic - International University of Sarajevo - Bosnia and Herzegovina
35. Assist. Prof. Dr. Murat Karakaya - Atılım University - Turkey
36. Assist. Prof. Dr. Sasan Rabieh - Shahid Beheshti University - Iran
37. Assist. Prof. Dr. Ševkija Okerić - University of Sarajevo - Bosnia and Herzegovina
38. Assist. Prof. Dr. Ivana Plazonić - University of Zagreb - Croatia
39. Assist. Prof. Dr. J. Amudhavel - VIT Bhopal University - India
40. Assist. Prof. Dr. Hasan Bora Usluer - Galatasaray University - Turkey
41. Dr. Muhammet Uzun - RWTH Aachen University - Germany
42. Dr. Zsolt Hetesi - National University of Public Service, Budapest - Hungary
43. Dr. Zsolt T. Németh - National University of Public Service, Budapest - Hungary

ORGANIZATION COMMITTEE

Chairman of the Conference

Prof. Dr. Özer Çınar – Yıldız Technical University - Turkey

Members of the Committee

Prof. Dr. M. Asghar Fazel – University of Environment - Iran

Prof. Dr. Ümit Alver - Karadeniz Technial University - Turkey

Assoc.Prof.Dr. Agim Mamuti - Mother Teresa University - North Macedonia

Assoc. Prof. Dr. Lukman Thalib - Qatar University - Qatar

Assoc. Prof. Dr. Nusret Drešković - University of Sarajevo - Bosnia and Herzegovina

Assist. Prof. Dr. Sasan Rabieh - Shahid Beheshti University - Iran

Alma Ligata - Zenith Group - Bosnia and Herzegovina

Ismet Uzun - Zenith Group - Bosnia and Herzegovina

Musa Kose - Zenith Group - Bosnia and Herzegovina

WELCOME TO ICETI 2022

On behalf of the organizing committee, we are pleased to announce that the International Conference On Engineering Technology And Innovation is held on eld on May 04-08, 2022 in Sarajevo, Bosnia and Herzegovina. ICETI 2022 provides an ideal academic platform for researchers to present the latest research findings and describe emerging technologies, and directions in Engineering Technology And Innovation. The conference seeks to contribute to presenting novel research results in all aspects of Engineering Technology And Innovation. The conference aims to bring together leading academic scientists, researchers and research scholars to exchange and share their experiences and research results about all aspects of Engineering Technology And Innovation. It also provides the premier interdisciplinary forum for scientists, engineers, and practitioners to present their latest research results, ideas, developments, and applications in al lareas of Engineering Technology And Innovation. The conference will bring together leading academic scientists, researchers and scholars in the domain of interest from around the world. ICETI 2022 is the oncoming event of the successful conference series focusing on Engineering Technology And Innovation. The International Conference on Engineering Technology and Innovation (ICETI 2022) aims to bring together leading academic scientists, researchers and research scholars to exchange and share their experiences and research results about all aspects of Engineering Technology and Innovation. It also provides the premier interdisciplinary forum for scientists, engineers, and practitioners to present their latest research results, ideas, developments, and applications in all areas of Engineering Technology and Innovation. The conference will bring together leading academic scientists, researchers and scholars in the domain of interest from around the world. The conference's goals are to provide a scientific forum for all international prestige scholars around the world and enable the interactive exchange of state-of-the-art knowledge. The conference will focus on evidence-based benefits proven in technology and innovation and engineering experiments.

Best regards,

Prof. Dr. Özer ÇINAR

Microstructural Evaluation and Mechanical Properties of 0.75% Vanadium-Alloyed Spheroidal Graphite Cast Iron

Acelya Sandikoglu Kandemir[1]*, Ridvan Gecu[2]

Abstract

Spheroidal graphite cast irons (SGCIs) have been widely used in automotive and energy industries owing to their unique microstructures consisting of graphite nodules in ferritic, pearlitic, or ferritic/pearlitic matrices. Alloying elements can be added to improve the mechanical strength of the SGCIs by changing the amount, size, volume, and distribution of the microstructural components. In this study, GGG40, also known as EN-GJS-400-15, grade spheroidal graphite cast iron was alloyed with 0.75% vanadium in an induction furnace, and its microstructural evolution and mechanical properties were investigated compared to the unalloyed commercial alloy. Both unalloyed and 0.75% V-alloyed ductile iron specimens fabricated by sand mold casting were examined by a light optical microscope equipped with image analysis software, a universal tensile test machine, and a Brinell hardness tester. The alteration in the volume, nodularity, count, size, and distribution of graphite, and the alteration in the ferrite/pearlite ratio, hardness, and tensile test results were discussed as a function of V content.

Keywords: Spheroidal graphite cast iron; alloying; vanadium; microstructural evolution

1. INTRODUCTION

Spheroidal graphite cast irons, which emerged at the end of the first half of the 20th century, are today referred to as the first generation in various sources. When looking at the microstructure of these first-generation cast irons containing approximately 2-3% silicon, it is seen that the matrix is composed of ferrite, perlite, or a mixture of both. While pearlite creates an effect that strengthens the material but reduces its ductility, ferrite allows obtaining a more ductile material. Therefore, by changing the pearlite and ferrite ratios in the structure, the desired hardness, strength, and elongation of the produced part values can be obtained [1]. The ratio of ferrite and pearlite is important to optimize mechanical properties in first-generation spheroidal graphite cast irons. The common problem in this type of cast iron is the formation of varying amounts of pearlite in sections of different thicknesses since the amount of pearlite in the structure changes not only depending on the chemical composition but also depending on the cooling rate. For this reason, while the ferrite ratio, which gives ductility to the structure, increases in slowly cooling thick sections of a cast piece with different section thicknesses, pearlite formation, which reduces ductility but strengthens the structure, is observed at a higher rate in fast cooling thin sections [2].

There has been an extensive research effort to develop micro-alloyed ductile iron in which small additions of elements such as niobium and vanadium provide significant increases in strength through grain size control and precipitation hardening. Since vanadium is a carbide stabilizer, it modifies the solidification of the metastable austenite/cementite system and therefore tends to promote the formation of eutectic carbide. Vanadium slightly encourages the formation of ferrite. When vanadium is added to cast iron, white inclusions with more or less random distribution are also observed in the microstructure. It was stated that the wear and hardness values increased, and the elongation values decreased with increasing vanadium values [3,4,5].

[1] *Ferro Dokum San. ve Dis Tic. A.S., Istanbul, Turkey*

[2] *Yildiz Technical University, Department of Metallurgical and Materials Engineering, Istanbul, Turkey*

In this study, microstructural evolution and the alteration in mechanical properties were investigated with the addition of 0.75% vanadium and the difference between thick and thin sections.

2. MATERIALS AND METHODS:

2.1. Fabrication

Charge materials composed of pig iron, steel scrap, and electrolytic copper were prepared and melted using a 100 kg capacity induction furnace. The melt was overheated at 1540 °C, and the determined amount of vanadium was added to the melt during furnace charging.

Following the treatment at 1540 °C, 1.4 wt.% FeSiMg5 as a modifier and 0.3 wt.% FeSi75 as an inoculant were added to the melt at 1400 °C.

Two ingots were fabricated with 0% and 0.75% vanadium. Following the production, the specimens for tensile and hardness tests and microscopic examinations were sectioned along the vertical central axis and machined to obtain the appropriate dimensions required from the tests.

Table 1: *Chemical compositions of V-alloyed nodular cast irons (wt%).*

C	Si	Mn	Cr	S	Cu	P	Mg	V
3.72	2.55	0.10	0.02	0.0014	0.15	0.042	0.06	0
3.8	2.5806	0.0926	0.0395	0.0177	0.0408	0.0375	0.0611	0.76

2.2. Characterization

Image analyzer software via optical microscopy was used to determine phase ratios, nodule counts, and graphite sizes.

Rectangular dog-bone-shaped samples with a gauge length of 50 mm and a width of 12.5 mm were subjected to tensile strength measurements using a universal tensile tester equipped with an axial extensometer. Two specimens were analyzed for each ductile iron alloyed with various amounts of vanadium, and the results were reported as an average of these tests.

A Brinell tester was used to measure the hardness of the samples after production. A load of 1839 N was applied by an indenter with a diameter of 2.5 mm during 10 s. Three random measurements were taken from each sample surface, and the average hardness values of these calculations were given.

3. RESULT AND DISCUSSION

3.1. Formed Phases

Fig. 1 shows the as-polished microstructures of the spheroidal graphite iron specimens. The cast iron demonstrated in Fig. 1a does not contain vanadium, whereas the samples in Fig. 1b and Fig. 1c are alloyed with 0.75% vanadium. The thickness values are 10mm for the thin section and 60 mm for the thick section. The ferritic/pearlitic matrix in white color is surrounded by the graphite particles in black color for all samples. When the micrographs were examined, it was observed that the nodularity decreased with increasing vanadium.

Vanadium, like many other elements, restricts the formation of austenite, causing the contraction in austenite in the Fe-C equilibrium diagram. It means that vanadium slightly encourages the ferrite formation by increasing the transformation temperature [6]. Fig. 2 demonstrates the optical microscope images of the samples etched with %2 Nital to reveal the ferrite/pearlite boundaries. The amounts of ferrite increased with increasing vanadium, while the graphite nodule counts increased, as given in Fig. 3.

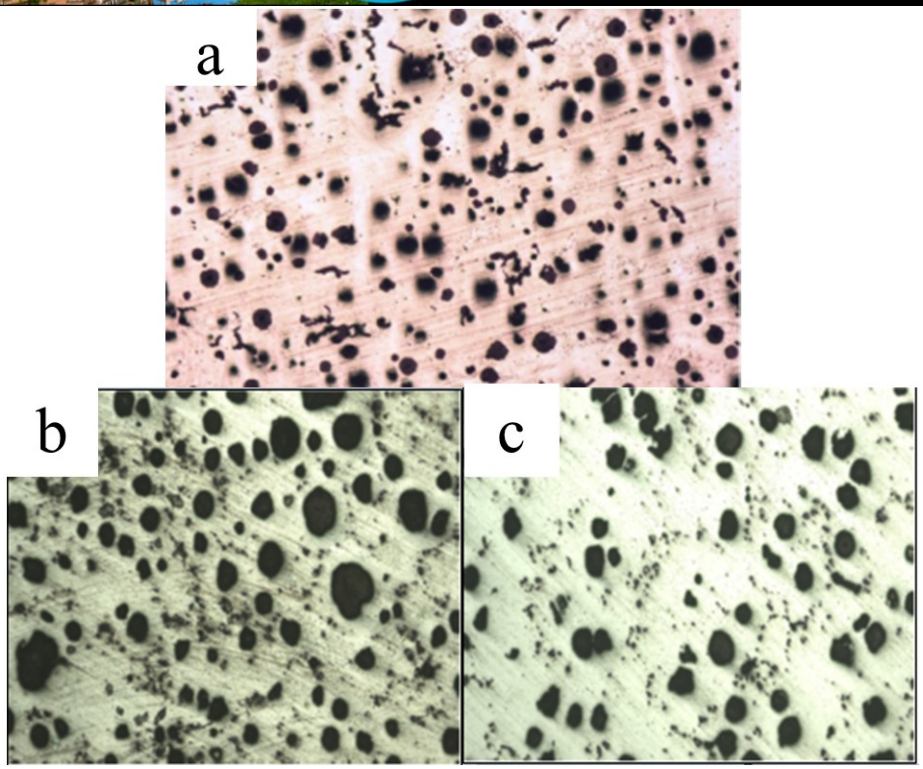

Figure 1: *As-polished microstructures of nodular cast irons alloyed with a) 0% V, b) 0.75% V thin section, and c) 0.75% V thick section*

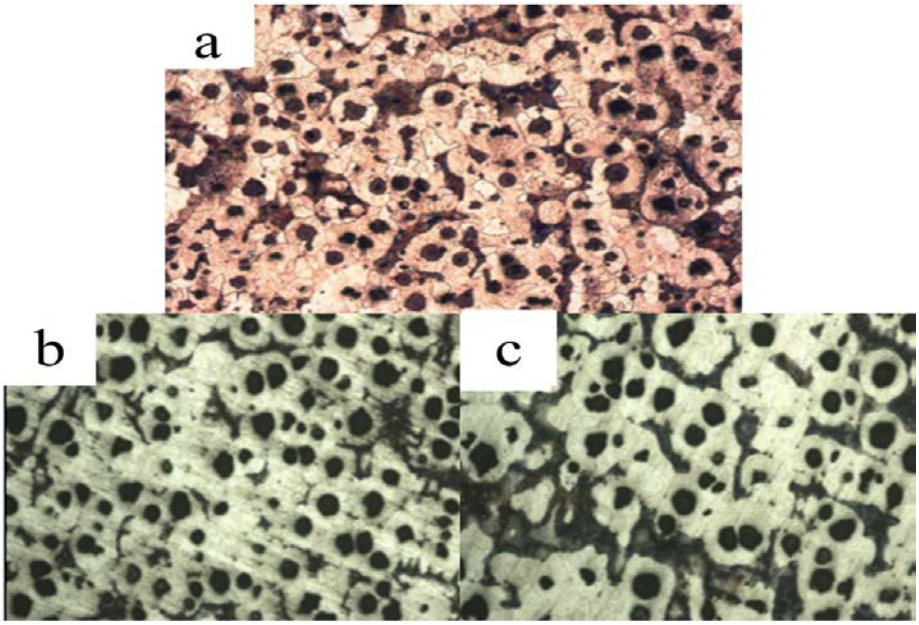

Figure 2: *Etched microstructures of nodular cast irons alloyed with a) 0% V, b) 0.75% V thin section, and c) 0.75% V thick section (etched with 2% Nital)*

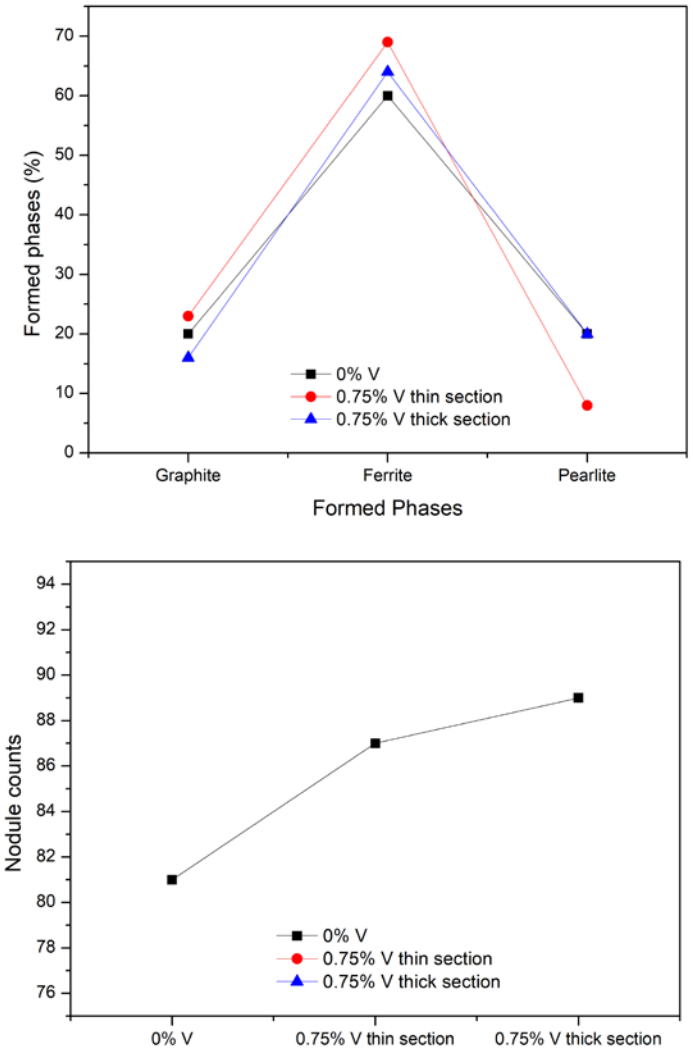

Figure 3: *Influence of amount of vanadium on the formed phases and nodules count*

Apart from the tendency of vanadium to promote eutectic iron carbide formation during solidification and its mild tendency to promote pearlite formation during eutectoid transformation, its addition to ductile iron caused the formation of an additional phase in the microstructure.

3.2. Mechanical Test Results

Figs. 4 and 5 show the average results of the ultimate tensile strength (UTS) and elongation. While the UTS of the samples with vanadium addition are close to each other, the difference between the elongation values is significant, as expected. This can be attributed to a reduction in the volume fraction of graphite and the presence of vanadium carbide particles.

The yield strength of ferrite was controlled by the grain size and solid solution strengthening, whereas the yield strength of pearlite was a function of the interlamellar spacing, colony size, cementite plate thickness, and solid solution strengthening of the ferrite.

Hence apart from the effect of vanadium carbide particles on decreasing the ferrite grain size, vanadium also improves the yield strength by increasing the volume fraction of pearlite. The reduction in total elongation of

ductile iron as increased vanadium content (Fig. 5) can be attributed to the increased volume fractions of second phase particles (vanadium carbide) and pearlite.

The hardness results are given in Fig 6. The results are associated with the tensile strength values. The hardness values were higher in the thin section than the thick section, although vanadium addition provided better hardness for both specimens compared to the unalloyed sample.

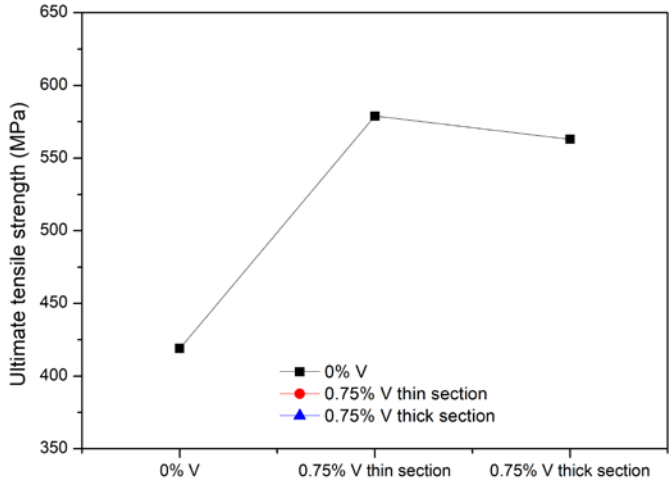

Figure 4: *Influence of vanadium on ultimate tensile strength*

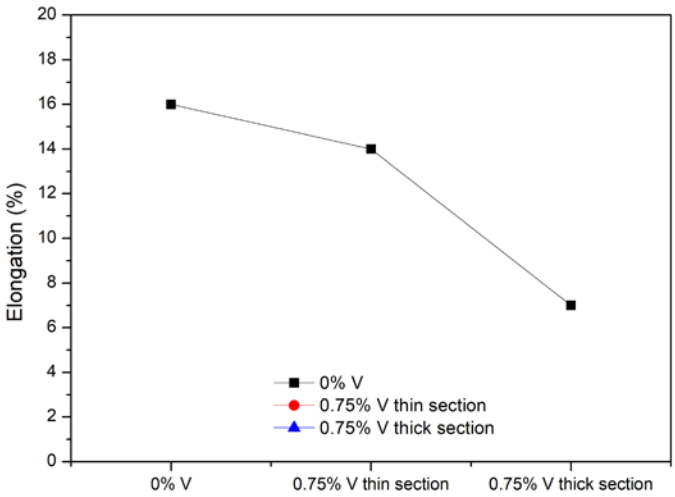

Figure 5: *Influence of vanadium on elongation*

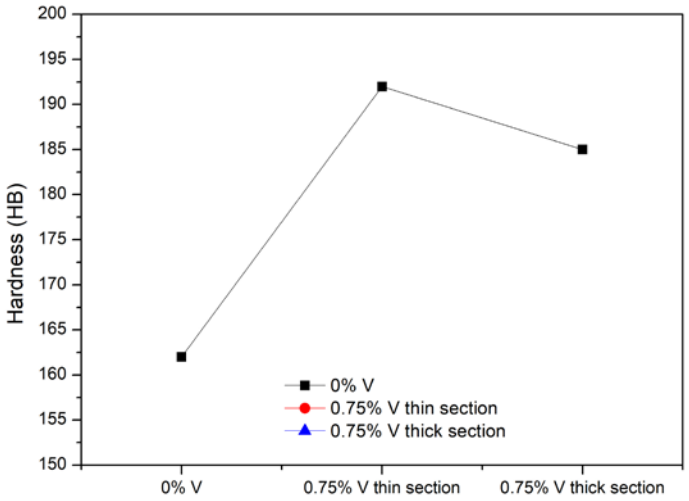

Figure 6: *Influence of vanadium on hardness results*

4. CONCLUSIONS

The following conclusions were found from the microstructural and mechanical characterization.

- As the vanadium content in iron increased, the ultimate tensile strength increased while the elongation decreased.
- Hardness values increased due to the carbide-forming effect of vanadium. Due to the cooling difference, thick-sectioned parts had lower hardness than the thin sections.
- Vanadium had a strong tendency to promote the formation of eutectic carbide in ductile iron. The ferrite content increased by the addition of 0.75% vanadium.
- The amount of nodularity has increased since vanadium acted as a spheroidizer in the cast irons.

REFERENCES

[1]. B. Duit, S. Degirmenci, B. Sirin. EN-1563 New generation ductile irons (Solid solution strengthened ductile irons). Proceedings of the Ankiros 7th InternationalFoundry Congress, 2014.
[2]. W. Stets, H. Loblich, G. Gassner, P. Schumacher. Solution strengthened ferritic ductile cast iron: Properties, production and application. 8th International Journal of Metalcasting, 2014.
[3]. A. S. Filippov, E. M. Blank and V. S. Iveliev, "Influence of vanadium additions on the structure and properties of irons". J. Russian Casting Production. 1969, 289-291.
[4]. T. Ohide and K. Ikawa, "Effect of vanadium on the as-cast and isothermally transformed structures of spheroidal graphite cast iron", J. Japan Foundrymen's Society, 1985, 57, 522-527. (2007)
[5]. S. B. Maselenkov. V. A. Teikh, G. I. Silman and V. K.Thomas, "Distribution of V, Mo, Cu, and W in cast iron", J. Russian Casting Production, 1969, 375-377.
[6]. M.Rezvani, J.Campbell, “The effect of vanadium in as-cast ductile iron”, International Journal of Cast Metals Research, 2017,1-15

Microstructural Evaluation and Mechanical Properties of 0.75% Vanadium-Alloyed Spheroidal Graphite Cast Iron

Acelya Sandikoglu Kandemir[1]*, Ridvan Gecu[2]

Abstract

Spheroidal graphite cast irons (SGCIs) have been widely used in automotive and energy industries owing to their unique microstructures consisting of graphite nodules in ferritic, pearlitic, or ferritic/pearlitic matrices. Alloying elements can be added to improve the mechanical strength of the SGCIs by changing the amount, size, volume, and distribution of the microstructural components. In this study, GGG40, also known as EN-GJS-400-15, grade spheroidal graphite cast iron was alloyed with 0.75% vanadium in an induction furnace, and its microstructural evolution and mechanical properties were investigated compared to the unalloyed commercial alloy. Both unalloyed and 0.75% V-alloyed ductile iron specimens fabricated by sand mold casting were examined by a light optical microscope equipped with image analysis software, a universal tensile test machine, and a Brinell hardness tester. The alteration in the volume, nodularity, count, size, and distribution of graphite, and the alteration in the ferrite/pearlite ratio, hardness, and tensile test results were discussed as a function of V content.

Keywords: Spheroidal graphite cast iron; alloying; vanadium; microstructural evolution

1. INTRODUCTION

Spheroidal graphite cast irons, which emerged at the end of the first half of the 20th century, are today referred to as the first generation in various sources. When looking at the microstructure of these first-generation cast irons containing approximately 2-3% silicon, it is seen that the matrix is composed of ferrite, perlite, or a mixture of both. While pearlite creates an effect that strengthens the material but reduces its ductility, ferrite allows obtaining a more ductile material. Therefore, by changing the pearlite and ferrite ratios in the structure, the desired hardness, strength, and elongation of the produced part values can be obtained [1]. The ratio of ferrite and pearlite is important to optimize mechanical properties in first-generation spheroidal graphite cast irons. The common problem in this type of cast iron is the formation of varying amounts of pearlite in sections of different thicknesses since the amount of pearlite in the structure changes not only depending on the chemical composition but also depending on the cooling rate. For this reason, while the ferrite ratio, which gives ductility to the structure, increases in slowly cooling thick sections of a cast piece with different section thicknesses, pearlite formation, which reduces ductility but strengthens the structure, is observed at a higher rate in fast cooling thin sections [2].

There has been an extensive research effort to develop micro-alloyed ductile iron in which small additions of elements such as niobium and vanadium provide significant increases in strength through grain size control and precipitation hardening. Since vanadium is a carbide stabilizer, it modifies the solidification of the metastable austenite/cementite system and therefore tends to promote the formation of eutectic carbide. Vanadium slightly encourages the formation of ferrite. When vanadium is added to cast iron, white inclusions with more or less random distribution are also observed in the microstructure. It was stated that the wear and hardness values increased, and the elongation values decreased with increasing vanadium values [3,4,5].

[1] *Ferro Dokum San. ve Dis Tic. A.S., Istanbul, Turkey*

[2] *Yildiz Technical University, Department of Metallurgical and Materials Engineering, Istanbul, Turkey*

In this study, microstructural evolution and the alteration in mechanical properties were investigated with the addition of 0.75% vanadium and the difference between thick and thin sections.

2. MATERIALS AND METHODS:

2.1. Fabrication

Charge materials composed of pig iron, steel scrap, and electrolytic copper were prepared and melted using a 100 kg capacity induction furnace. The melt was overheated at 1540 °C, and the determined amount of vanadium was added to the melt during furnace charging.

Following the treatment at 1540 °C, 1.4 wt.% FeSiMg5 as a modifier and 0.3 wt.% FeSi75 as an inoculant were added to the melt at 1400 °C.

Two ingots were fabricated with 0% and 0.75% vanadium. Following the production, the specimens for tensile and hardness tests and microscopic examinations were sectioned along the vertical central axis and machined to obtain the appropriate dimensions required from the tests.

Table 1: *Chemical compositions of V-alloyed nodular cast irons (wt%).*

C	Si	Mn	Cr	S	Cu	P	Mg	V
3.72	2.55	0.10	0.02	0.0014	0.15	0.042	0.06	0
3.8	2.5806	0.0926	0.0395	0.0177	0.0408	0.0375	0.0611	0.76

2.2. Characterization

Image analyzer software via optical microscopy was used to determine phase ratios, nodule counts, and graphite sizes.

Rectangular dog-bone-shaped samples with a gauge length of 50 mm and a width of 12.5 mm were subjected to tensile strength measurements using a universal tensile tester equipped with an axial extensometer. Two specimens were analyzed for each ductile iron alloyed with various amounts of vanadium, and the results were reported as an average of these tests.

A Brinell tester was used to measure the hardness of the samples after production. A load of 1839 N was applied by an indenter with a diameter of 2.5 mm during 10 s. Three random measurements were taken from each sample surface, and the average hardness values of these calculations were given.

3. RESULT AND DISCUSSION

3.1. Formed Phases

Fig. 1 shows the as-polished microstructures of the spheroidal graphite iron specimens. The cast iron demonstrated in Fig. 1a does not contain vanadium, whereas the samples in Fig. 1b and Fig. 1c are alloyed with 0.75% vanadium. The thickness values are 10mm for the thin section and 60 mm for the thick section. The ferritic/pearlitic matrix in white color is surrounded by the graphite particles in black color for all samples. When the micrographs were examined, it was observed that the nodularity decreased with increasing vanadium.

Vanadium, like many other elements, restricts the formation of austenite, causing the contraction in austenite in the Fe-C equilibrium diagram. It means that vanadium slightly encourages the ferrite formation by increasing the transformation temperature [6]. Fig. 2 demonstrates the optical microscope images of the samples etched with %2 Nital to reveal the ferrite/pearlite boundaries. The amounts of ferrite increased with increasing vanadium, while the graphite nodule counts increased, as given in Fig. 3.

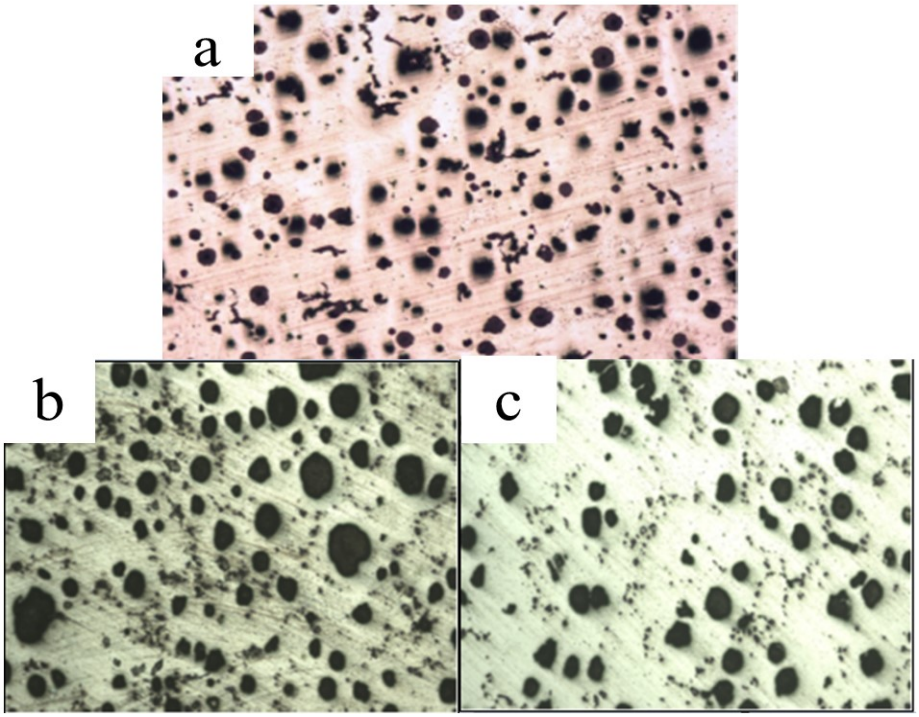

Figure 1: *As-polished microstructures of nodular cast irons alloyed with a) 0% V, b) 0.75% V thin section, and c) 0.75% V thick section*

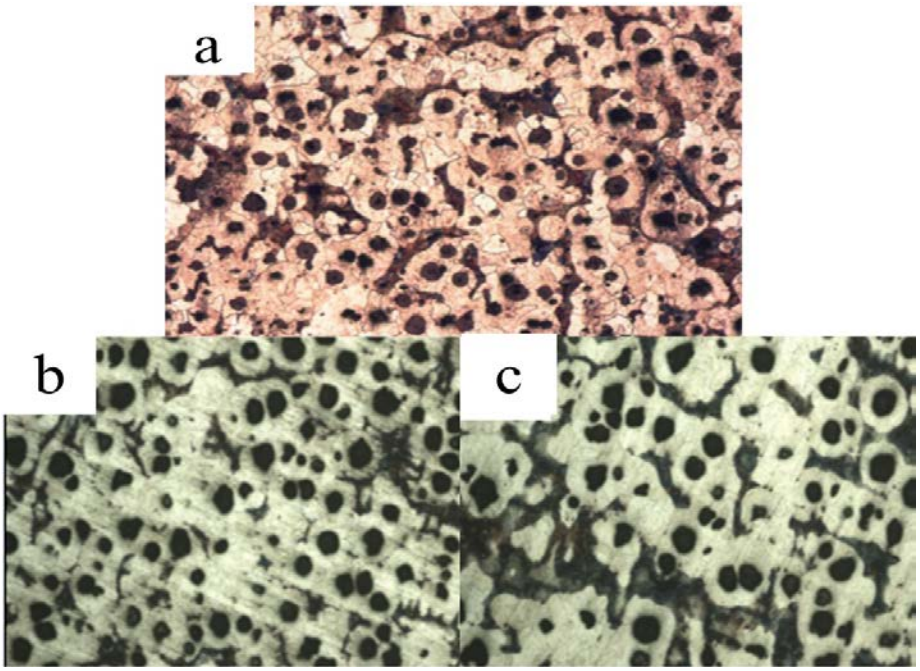

Figure 2: *Etched microstructures of nodular cast irons alloyed with a) 0% V, b) 0.75% V thin section, and c) 0.75% V thick section (etched with 2% Nital)*

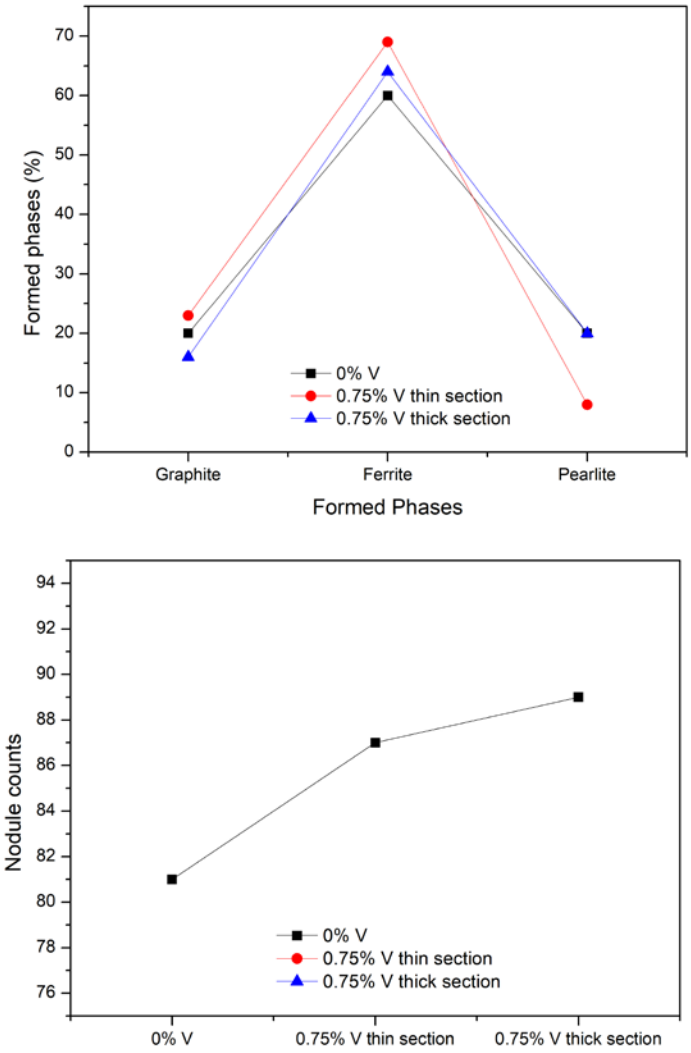

Figure 3: *Influence of amount of vanadium on the formed phases and nodules count*

Apart from the tendency of vanadium to promote eutectic iron carbide formation during solidification and its mild tendency to promote pearlite formation during eutectoid transformation, its addition to ductile iron caused the formation of an additional phase in the microstructure.

3.2. Mechanical Test Results

Figs. 4 and 5 show the average results of the ultimate tensile strength (UTS) and elongation. While the UTS of the samples with vanadium addition are close to each other, the difference between the elongation values is significant, as expected. This can be attributed to a reduction in the volume fraction of graphite and the presence of vanadium carbide particles.

The yield strength of ferrite was controlled by the grain size and solid solution strengthening, whereas the yield strength of pearlite was a function of the interlamellar spacing, colony size, cementite plate thickness, and solid solution strengthening of the ferrite.

Hence apart from the effect of vanadium carbide particles on decreasing the ferrite grain size, vanadium also improves the yield strength by increasing the volume fraction of pearlite. The reduction in total elongation of

ductile iron as increased vanadium content (Fig. 5) can be attributed to the increased volume fractions of second phase particles (vanadium carbide) and pearlite.

The hardness results are given in Fig 6. The results are associated with the tensile strength values. The hardness values were higher in the thin section than the thick section, although vanadium addition provided better hardness for both specimens compared to the unalloyed sample.

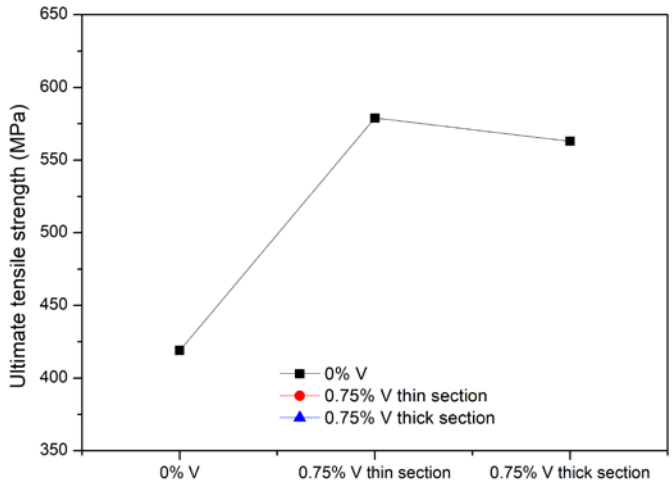

Figure 4: *Influence of vanadium on ultimate tensile strength*

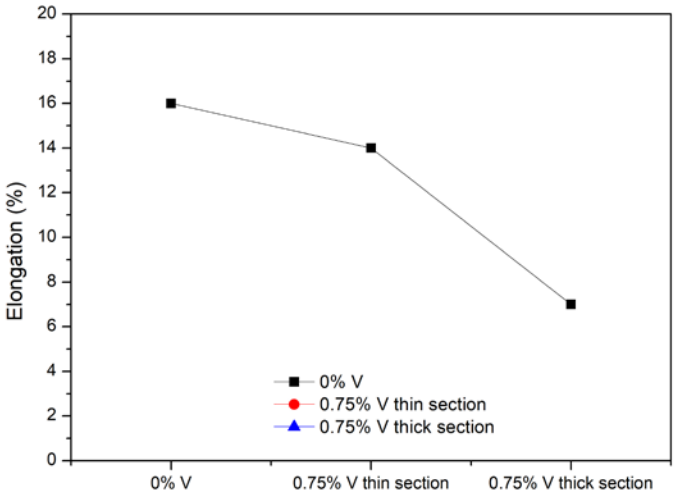

Figure 5: *Influence of vanadium on elongation*

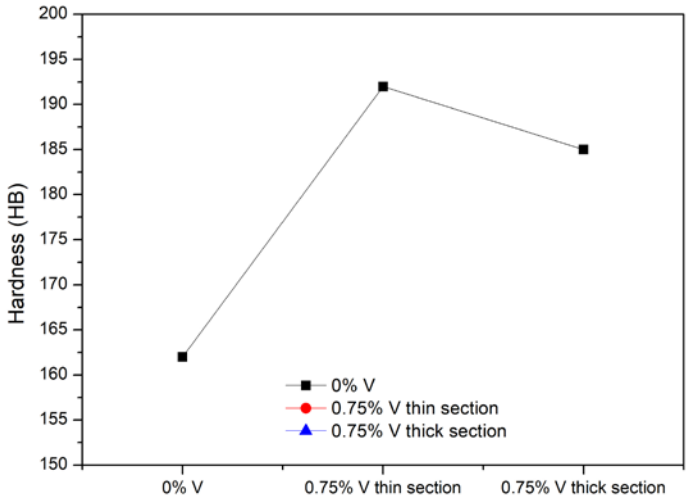

Figure 6: *Influence of vanadium on hardness results*

4. CONCLUSIONS

The following conclusions were found from the microstructural and mechanical characterization.

- As the vanadium content in iron increased, the ultimate tensile strength increased while the elongation decreased.
- Hardness values increased due to the carbide-forming effect of vanadium. Due to the cooling difference, thick-sectioned parts had lower hardness than the thin sections.
- Vanadium had a strong tendency to promote the formation of eutectic carbide in ductile iron. The ferrite content increased by the addition of 0.75% vanadium.
- The amount of nodularity has increased since vanadium acted as a spheroidizer in the cast irons.

REFERENCES

[1]. B. Duit, S. Degirmenci, B. Sirin. EN-1563 New generation ductile irons (Solid solution strengthened ductile irons). Proceedings of the Ankiros 7th InternationalFoundry Congress, 2014.
[2]. W. Stets, H. Loblich, G. Gassner, P. Schumacher. Solution strengthened ferritic ductile cast iron: Properties, production and application. 8th International Journal of Metalcasting, 2014.
[3]. A. S. Filippov, E. M. Blank and V. S. Iveliev, "Influence of vanadium additions on the structure and properties of irons". J. Russian Casting Production. 1969, 289-291.
[4]. T. Ohide and K. Ikawa, "Effect of vanadium on the as-cast and isothermally transformed structures of spheroidal graphite cast iron", J. Japan Foundrymen's Society, 1985, 57, 522-527. (2007)
[5]. S. B. Maselenkov. V. A. Teikh, G. I. Silman and V. K.Thomas, "Distribution of V, Mo, Cu, and W in cast iron", J. Russian Casting Production, 1969, 375-377.
[6]. M.Rezvani, J.Campbell, “The effect of vanadium in as-cast ductile iron”, International Journal of Cast Metals Research, 2017,1-15

Effect of water-reducing admixture main chain length change on consistency retention performance of mortar mixtures having different C_3A content

Veysel Kobya[1], Kemal Karakuzu[1], Ali Mardani[1]*

Abstract

In this study, the effect of the PCE main chain length variation on the admixture demand to provide the desired slump value (27±2 cm) and the consistency retention performance of mortar mixtures having different C_3A content was investigated. For this purpose, a total of 12 mortar mixtures were prepared by using CEM I 42.5R type cement having four different C_3A content (2%, 3%, 6%, 9%) and using PCEs having three different main chain lengths (27000 g/mol, 55500 g/mol, 78000 g/mol). According to the results, irrespective of the PCE type, the PCE requirement increased by an increment of the C3A ratio. This behaviour was more pronounced in the mixture containing the cement having the highest C_3A ratio (9%). Compared to the mixture containing PCE having medium main chain length, the admixture demand to provide desired slump value of mixture containing PCEs having short and long main chains was obtained 3.9-4.5 and 4.7-6.5 times higher, respectively. The shortness of the PCE's main chain reduces the adsorption and electrostatic effect of the admixture. The poor performance of the PCE having a long main chain may be due to the bridging effect and the intertwining of the long polymers. PCE having a medium main chain showed almost %21 lower consistency retention performance than the other ones. This is due to the greater admixture requirement to achieve target flow value in the mixtures containing admixture with short and long main chains compared to admixtures with medium chains.

Keywords: C_3A, consistency retention performance, main chain length, PCE, PCE requirement

1. INTRODUCTION

Polycarboxylate-based water-reducing admixtures (PCE) consist of the main chain having carboxylic groups and comb-like side chains with polyethylene groups terminated by hydroxyl or methyl. The chain properties of PCEs are one of the most important parameters affecting their dispersing performance [1-5]. Electrostatic repulsion results from the anionic monomers that are adsorbed on the surface of the cement grains due to the negatively charged main chain. Therefore, cement particle agglomeration is avoided. Furthermore, because of steric hindrance, non-ionic polyethylene glycol (PEG) side chains repulse cement granules physically, increasing fluidity [6,7]. While adsorption is determined by the number of free carboxylate groups (COO^-), steric hindrance is determined by the adsorbed polymer's side chain characteristics [8-10].

The number of carboxylate groups on the main chain increment as the PCE main chain length increases. Consequently, an increment in adsorption is expected. On the other hand, PCE's efficiency is reduced by a bridging effect caused by long main chains or larger polymer molecules. Because of the bridging effect, cement particles flocculate, decreasing the workability (fluidity) of mixtures. The bridging effect occurs when a PCE molecule attaches to more than one cement particle [11,12].

C_3A content of cement is one of the most important parameters affecting PCE efficiency because C_3A is the most reactive component of cement. Its high reactivity has a significant impact on PCE's performance.

[1] *Corresponding author:*
Department of Civil Engineering, Bursa Uludag University, Bursa, Turkey, ali.mardani16@gmail.com

Furthermore, negatively charged PCE molecules have a strong attraction to the positively charged surface of C_3A and its hydration products (calcium sulfoaluminate hydrates) [2]. Rapid hydration and hence low rheological performance (high yield stress and apparent viscosity) are provided by high C_3A cement paste. Besides, a high C_3A amount causes low consistency retention performance and high PCE requirement [13,14]

In this study, the effect of the PCE main chain length change on the PCE requirement and the consistency retention performance of mortar mixtures having different C_3A content was investigated.

2. MATERIALS AND METHODS

Within the scope of the study, CEMI 42.5R type Portland cement having four different C_3A content, in accordance with the EN 197-1, was utilized. Cements and PCEs are nominated as their C_3A contents and molecular weights (Table 1). Standard CEN sand in accordance with EN 196-1 was utilized as aggregate. The specific gravity and water absorption rate of the sand are 2.72 and 0.7%, respectively.

Table 1. Cements and PCEs nomination

Cement and PCE nomination	C_3A content (%)	Molecular weight (g/mol)
C2	2.13	-
C3	3.60	-
C6	6.82	-
C9	9.05	-
PCE27k	-	27000
PCE55k	-	55500
PCE78k	-	78000

All mortar mixtures were prepared in accordance with ASTM C109 and the w/c ratio, sand/cement ratio and slump value were kept constant as 0.485, 2.75 and 27±2 cm, respectively. The PCE requirement to provide the desired slump value was determined in accordance with ASTM C1437. Besides, consistency retention performances were measured at every 15 min for 1 hour.

3. RESULT AND DISCUSSION

Time-dependent slump-flow value and relative PCE requirement for desired slump value of all mortar mixtures are given in Table 2. Mixtures are nominated based on the cement used and admixture. For instance, the mixture containing C2 cement and PCE27k admixture is named as C2PCE27k.

As it seen from Table 2, regardless of the PCE type, the PCE requirement increased with the increment in cement C_3A content. The increase in the PCE requirement is more evident in the mixtures prepared with C9 cement. Similar results were found in previous studies regarding the negative effects of C_3A on the fresh properties of cementitious systems [13,15-16].

The PCE requirement for desired slump value of PCE27k and PCE 78k were obtained 3.9-4.5 and 4.7-6.5 times higher than that of the PCE 55k, respectively. It was attributed to the PCE having a short main chain (PCE 27k) resulting in a decrease in adsorption and electrostatic repulsion [6]. For the PCE having long main chain (PCE 78k), it may occur due to the bridging effect and the intertwining of the polymers. Cement particles flocculate and consequently workability (fluidity) of the mixtures reduce due to bridging effect.

PCE55k showed almost %21 lower consistency retention performance than PCE27k and PCE78k. This was attributed to the fact that the PCE requirements for the target slump value of PCE having short and long main chain were much higher than for the PCE having medium main chain length (PCE55k). As a result, the non-adsorbed part of PCE27k and PCE78k may higher than PCE55k. As it is known, the non-adsorbed part of PCE determines fluidity properties such as time-dependent consistency retention behavior [12,14].

Table 2. Time-dependent slump performance of mixtures

		Time-dependent slump value (cm)				
Mixtures	**Relative PCE ratio (%)**	**0 min.**	**15 min.**	**30 min.**	**45 min.**	**60 min.**
C2-PCE27k	100	27	24.5	23.5	22	21.6
C2-PCE55k	20.3	26.8	19.2	18.8	17.6	17.5
C2-PCE78k	116.4	26.9	24.1	23	22.6	22.2
C3-PCE27k	100	26.9	24.1	22.5	22	20.9
C3-PCE55k	20	27.8	20.9	19	18	17.7
C3-PCE78k	116.9	26.6	23.7	22.8	21.7	21.2
C6-PCE27k	100	27	23.6	22.5	21.7	20.5
C6-PCE55k	20	27.9	21	19.1	17.9	17.6
C6-PCE78k	122.2	26.5	23.4	21.7	20.9	20.5
C9-PCE27k	100	26.9	22.3	21.5	20.4	19.1
C9-PCE55k	21.4	28	20.8	18.8	17.3	16.8
C9-PCE78k	127.5	27.4	22.5	21	20.5	18.9

4. CONCLUSION

In this study, the effect of the main chain length on the PCE requirement and the consistency retention performance of cementitious systems having different C_3A content was examined. The results are listed below:

- PCE having medium main chain length (55000 g/mol) outperformed the PCE having short main chain length (27000 g/mol) and long main chain length (78000 g/mol) in terms of PCE requirement for desired slump value.
- PCE having long main chain length was the worst PCE in terms of slump-flow performance and PCE requirement.
- PCE having short and long main chain length showed higher performance than PCE having medium main chain length in terms of consistency retention due to their use in high dosages.

In conclusion, it was determined that PCE with medium main chain length was the most suitable admixture in all mixtures having different C_3A ratio.

ACKNOWLEDGMENT

The authors gratefully acknowledge the support of the Bursa Uludag University Science and Technology Centre (BAP) under grant numbers FDK -2022/804 and the Scientific and Technological Research Council of Turkey (TUBITAK) (Grant No: 219 M425). The first author acknowledges the scholarships provided by the TUBITAK 2211A during his doctoral studies. In addition, the first and second authors acknowledge the scholarship provided by Turkish Council of Higher Education (YOK 100/2000 Program) during their PhD studies.

REFERENCES

[1] Ouyang, X., Jiang, X., Qiu, X., Yang, D., & Pang, Y. (2009). Effect of molecular weight of sulfanilic acid-phenol-formaldehyde condensate on the properties of cementitious system. Cement and Concrete Research, 39(4), 283-288.

[2] He, Y., X. Zhang, and R. D. Hooton. (2017). Effects of organosilane modified polycarboxylate superplasticizer on the fluidity and hydration properties of cement paste. Construction and Building Materials, 132:112–123.

[3] Sonebi, M., Lachemi, M. and Hossain, K.M.A. (2013). Optimization of rheological parameters and mechanical properties of superplasticized cement grouts containing metakaolin and viscosity modifying admixture. Construction and Building Materials, 38:126-38.

[4] Mardani-Aghabaglou, A., Tuyan, M., Yilmaz, G., Arioz, O., & Ramyar, K. (2013). Effect of different types of superplasticizers on fresh, rheological and strength properties of self-consolidating concrete. Construction and Building Materials, 47, 1020-1025.

[5] Altun, M. G., Ozen, S., & Mardani-Aghabaglou, A. (2020). Effect of side chain length change of polycarboxylate-ether based high range water reducing admixture on properties of self-compacting concrete. Construction and Building Materials, 246, 118427.

[6] Sha, S., Wang, M., Shi, C., & Xiao, Y. (2020). Influence of the structures of polycarboxylate superplasticizer on its performance in cement-based materials-A review. Construction and Building Materials

[7] Xiang, S., Gao, Y., & Shi, C. (2020). Progresses in synthesis of polycarboxylate superplasticizer. Advances in Civil Engineering, 2020, 8810443,14 pp.

[8] Nawa, T., Ichiboji, H., Kinoshita, M., (2000). Influence of temperature on fluidity of cement paste containing superplasticizer with polyethylene oxide graft chains. In: 6th CANMET/ACI International Conference on Superplasticizers and Other Chemical Admixtures in Concrete, 195, pp. 181e194.

[9] Flatt, R. J., Schober, I., Raphael, E., Plassard, C., & Lesniewska, E. (2009). Conformation of adsorbed comb copolymer dispersants. Langmuir, 25(2), 845-855.

[10] Erzengin, S. G., Kaya, K., Ozkorucuklu, S. P., Ozdemir, V., & Yildirim, G. (2018). The properties of cement systems superplasticized with methacrylic ester-based polycarboxylates. Construction and Building Materials, 166, 96-109.

[11] Kashani, A., Provis, J.L., Xu, J., Kilcullen, A.R., Qiao, G.G., & van Deventer, J. S. (2014). Effect of molecular architecture of polycarboxylate ethers on plasticizing performance in alkali-activated slag paste. Journal of Materials Science, 49(7), 2761-2772.

[12] Zhang, Q., Shu, X., Yu, X., Yang, Y., & Ran, Q. (2020). Toward the viscosity reducing of cement paste: Optimization of the molecular weight of polycarboxylate superplasticizers. Construction and Building Materials, 242, 117984.

[13] Zhang, S., Xu, X., Memon, S. A., Dong, Z., Li, D., & Cui, H. (2018). Effect of calcium sulfate type and dosage on properties of calcium aluminate cement-based self-leveling mortar. Construction and Building Materials, 167, 253-262.

[14] Karakuzu, K., Kobya, V., Mardani-Aghabaglou, A., Felekoglu, B., & Ramyar, K. (2021). Adsorption properties of polycarboxylate ether-based high range water reducing admixture on cementitious systems: A review. Construction and Building Materials, 312, 125366.

[15] Plank, J., & Hirsch, C. (2007). Impact of zeta potential of early cement hydration phases on superplasticizer adsorption. Cement and Concrete Research, 37(4), 537-542.

[16] Zingg, A., Winnefeld, F., Holzer, L., Pakusch, J., Becker, S., Figi, R., & Gauckler, L. (2009). Interaction of polycarboxylate-based superplasticizers with cements containing different C3A amounts. Cement and Concrete Composites, 31(3), 153-162

Effect of Shrinkage-Reducing Admixture Type and Utilization Rate on Shrinkage Behavior and Compressive Strength of Mortar Mixtures

Mustafa Kanat[1], Ali Mardani[1]*

Abstract

It is known that shrinkage behaviour is one of the most important parameters affecting the dimensional stability performance of cementitious systems. Nowadays, various methods are applied to prevent the shrinkage formation. It was found to be that the most common method is the addition of fiber and/or shrinkage-reducing admixtures (SRA) to the mixture. In this study, the effect of type and utilization rates of SRA on some fresh and hardened state properties of cementitious systems was investigated. For this purpose, a total of 10 mortar mixtures were prepared by adding neopentyl glycol (NG)-, hexylene glycol (HG)- and polypropylene glycol (PG)-based SRA to the control mixture at the ratios of 0.5%, 1% and 2% by weight of cement. CEM I 42.5R type cement and 0-4 mm crushed limestone aggregate were used. In all mixtures, the water/cement ratio and the slump value were kept constant. In order to provide the desired slump value, a polycarboxylate-ether based high-rate water reducing admixture (PCE) was used in different dosages. According to the results, irrespective of the SRA type, the flow performance and drying-shrinkage behavior of the mixtures were positively affected by the increment in the SRA utilization rate. It was observed that the 7-day compressive strength value of the mixtures decreased with the presence of SRA in the systems. This behavior was more pronounced by increasing the SRA utilization rate. It was understood that the negative effect on the compressive strength of SRA decreased with the increase of the curing time.

Keywords: Compressive strength, Dimensional stability, Shrinkage-reducing admixture, Slump value

1. INTRODUCTION

One of the various reasons affecting the durability performance of cementitious mixtures is the formation of cracks. It is known that one of the most important causes of crack formation is drying-shrinkage [1]. Drying-shrinkage occurs as a result of evaporation in an environment of insufficient humidity, under high temperature and wind conditions [2, 3]. Evaporation of free and adsorbed water in the concrete causes the formation of meniscus in the pores of the concrete [4, 5]. This meniscus, which is formed due to the surface tension of the water, tries to pull the pore walls inward and creates a shrinkage stress. In concretes with low tensile strength, shrinkage cracks occur due to these stresses [6]. Shrinkage cracks increase the permeability of cementitious mixtures and facilitate the entry of harmful substances. As a result, the durability performance of the mixtures decreases [1].

Shrinkage-reducing admixtures (SRA), pre-wetted lightweight aggregates, fibers and superabsorbent polymers are generally used to reduce drying-shrinkage [7]. The use of SRA is superior to the other methods due to its high shrinkage reduction and practicality. The effect of SRA on the drying-shrinkage behavior is attributed to the pore

[1] *Mustafa Kanat: Bursa Uludag University, Department of Civil Engineering, 16110, Nilufer/Bursa, Turkey.* 502126020@ogr.uludag.edu.tr

* *Corresponding author: Ali Mardani: Bursa Uludag University, Department of Civil Engineering, 16110, Nilufer/Bursa, Turkey.* alimardani@uludag.edu.tr

solution reducing the surface tension and increasing the internal relative humidity [8–10]. On the other hand, it was reported in previous studies that SRA prolongs the setting time and decreases the early age strength [11–13].

Mehdipour et al. [14] investigated the effect of using SRA on setting time, compressive strength and drying-shrinkage behavior of cementitious systems. According to the results, the use of SRA had a positive effect on the drying-shrinkage performance of the mixtures, however, it delayed the initial and final setting time and decreased the strength of the mixtures. Mardani et al. [15] investigated the effect of the use of SRA on the compressive strength and drying shrinkage behavior of mortar mixtures. They reported that the use of SRA decreased the early age compressive strength of mortar mixtures, however increased the 28-day compressive strength. On the other hand, it was observed that the SRA utilization has a positive effect on the drying-shrinkage performance of mortar mixtures.

In the literature, it was seen that glycol ether or polypropylene glycol-based admixtures are mostly used as SRA [16]. However, there is a few studies comparing the shrinkage and mechanical performance of different types of SRAs in the same cementitious system. In this study, the effect of using different types and ratios of SRA on some fresh and hardened state properties of cementitious systems was investigated. For this purpose, the effect of different types of SRAs at 0.5%, 1% and 2% ratios on the drying-shrinkage behavior and compressive strength of mortar mixtures were investigated.

2. MATERIAL and METHOD

2.1. Material

In the scope of the study, CEM 42.5 R type cement was used as binder. The chemical composition, physical and mechanical properties of the cement are given in Table 1.

Table 1. Chemical composition, physical and mechanical properties of cement

Oxide	**(%)**
SiO_2	19.30
Al_2O_3	4.38
Fe_2O_3	3.74
CaO	64.18
MgO	1.68
SO_3	2.78
Na_2O+0.658 K_2O	0.43
Cl^-	0.01
Insoluble residue	0.35
Loss on ignition	2.86
Free CaO	1.90

Physical properties		
Specific gravity		3.18
Blaine specific surface (cm^2/g)		4345
Mechanical properties		
Compressive Strength (MPa)	1-day	23.80
	2-day	33.60
	7-day	48.10

Crushed limestone aggregate was utilized as an aggregate. The specific gravity and water absorption rate of the sand are 2.64 and 1.1%, respectively. Polycarboxylate-ether based high-rate water reducing admixture (PCE) was used to achieve the target slump values. Within the scope of the study, three different glycol-based SRAs were used: hexylene glycol (HG), neopentyl glycol (NG) and polypropylene glycol (PG). Some chemical properties of SRA and PCE used are shown in Table 2.

Table 2. Some chemical properties of the admixtures used

Admixture type	Alkali content (%)	Density (g / cm ^{3})	Solid content (%)	Chloride content (%)	pH
NG	<10	1.06	99.9	<0.1	6.1
HG	<10	0.92	99.9	<0.1	6.4
PG	<10	1.00	99.9	<0.1	6.0
PCE	<10	1.06	32.0	<0.1	4.0

2.2. Method

In all mixtures, the water/cement ratio and the slump value were kept constant as 0.38 and 220±20 mm, respectively. A total of 10 mortar mixtures were prepared, one of which was a control mixture without SRA, and the other mixtures containing 0.5%, 1%, and 2% of SRA by weight of cement. The denomination of the mixtures was made according to the type of SRA and the utilization rate. For example, the mixture containing 1% HG was named as HG1. The amount of material used in the production of 1 dm^3 mortar mixes is given in Table 3.

Table 3. Theoretical mixing ratio for 1 dm^3 mortar mixes

Mixture	Cement (gr)	Crushed limestone aggregate (gr)	Water (gr)	SRA (%) *
C	544.7	1601.7	207.0	0
NG05	544.7	1594.9	207.0	0.5
NG1	544.7	1588.2	207.0	1.0
NG2	544.7	1574.7	207.0	2.0
HG05	544.7	1593.9	207.0	0.5
HG1	544.7	1586.1	207.0	1.0
HG2	544.7	1570.4	207.0	2.0
PG05	544.7	1594.5	207.0	0.5
PG1	544.7	1587.3	207.0	1.0
PG2	544.7	1572.9	207.0	2.0

*By weight of cement

Slump-flow values and compressive strengths of mortar mixtures were determined in accordance with ASTM C1437 and ASTM C109 Standards, respectively. The drying-shrinkage behavior of mortar mixtures was investigated in accordance with ASTM C596 Standard. For the drying-shrinkage measurement, 4 specimens with dimension of 25x25x285 mm were prepared from each mixture. The specimens prepared to examine the drying-shrinkage behavior were stored in the mold at 20°C and 95% relative humidity for 24 hours. The specimens removed from the mold were cured in lime-saturated water at 20°C for 48 hours. Then they kept in the cabinet where the temperature and relative humidity were 20°C and 55%, respectively, until the test day. The length variation of the specimens was calculated using Equation 1.

$$S = \left(\frac{L1-L}{L0}\right) \times 100 \quad (1)$$

Here, S is the shrinkage percentage of the sample, L_1 is the initial measurement value after it is removed from the curing pool, L is the periodic measurement value according to the elapsed days, L_0 is the effective measurement length.

3. RESULTS and DISCUSSION

3.1. Slump-flow performance

The PCE requirement is given in Table 4 to achieve a target slump value of 220±20 mm in mortar mixes. Regardless of the SRA type and utilization rate, the PCE requirement for the target slump value of the mixtures decreased with the addition of SRA. This situation became more evident with the increase in the use of SRA, regardless of the SRA type.
Among the SRA types, the mixtures containing NG and PG exhibited the highest and lowest performance in terms of slump-flow performance, respectively. The positive effect of the use of SRA on the slump-flow performance of cementitious systems has also been observed in previous studies [17, 18].

Table 4. Slump-flow values and PCE requirements of mixtures

Mixture	Slump-flow (cm)	PCE (%)*
C	20.75	0.85
NG05	24.00	0.75
NG1	23.00	0.70
NG2	21.00	0.60
HG05	23.50	0.80
HG1	23.25	0.75
HG2	24.00	0.70
PG05	23.00	0.80
PG1	22.25	0.80
PG2	22.75	0.75

* By weight of cement

3.2. Drying-Shrinkage Behavior

The drying-shrinkage values of the mortar mixtures exposed to drying-shrinkage for 28 days are shown in Figure 1. In addition, the relative drying-shrinkage values of the mixtures containing SRA compared to the control mixture are shown in Figure 2. Regardless of the type of SRA and the rate of utilization, the drying-shrinkage behavior of the mixtures was positively affected by the utilization of SRA. In addition, the amount of shrinkage decreases with the increase in the utilization rate of SRA. In this context, the mixtures containing NG admixture exhibited the weakest performance in terms of drying-shrinkage behavior. It was found that the other two types of SRA performed similarly in terms of shrinkage behavior.
Collepardi et al. [18] stated that the utilization of SRA increased the shrinkage performance in cementitious systems due to two effects. First, the tensile stresses arising from the meniscus formed by the surface tension of the water were reduced by the utilization of SRA. Second, due to the fact that SRA increased the viscosity of the pore solution and reduced moisture diffusion.

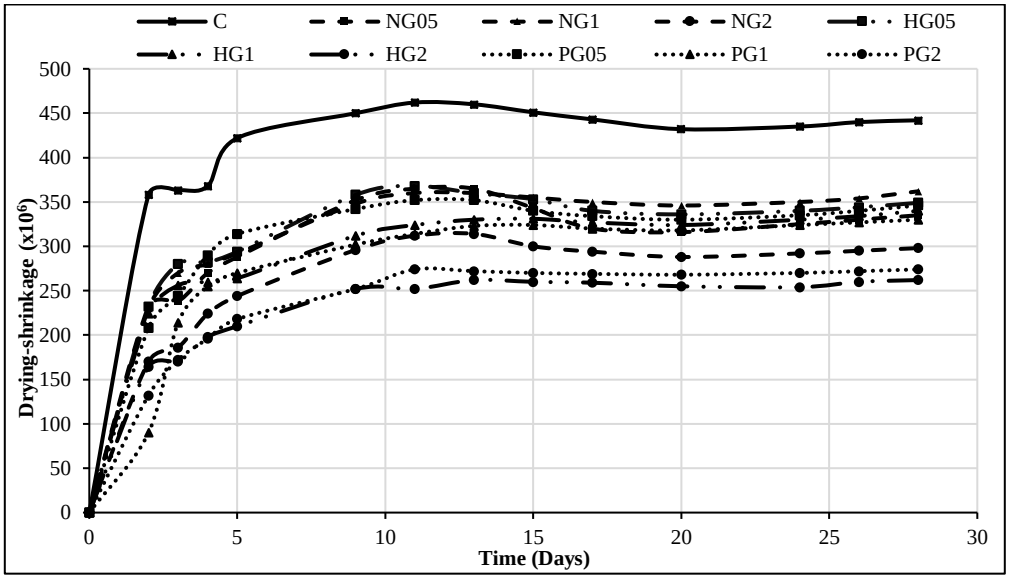

Figure 1. 28-day shrinkage behavior of mixtures

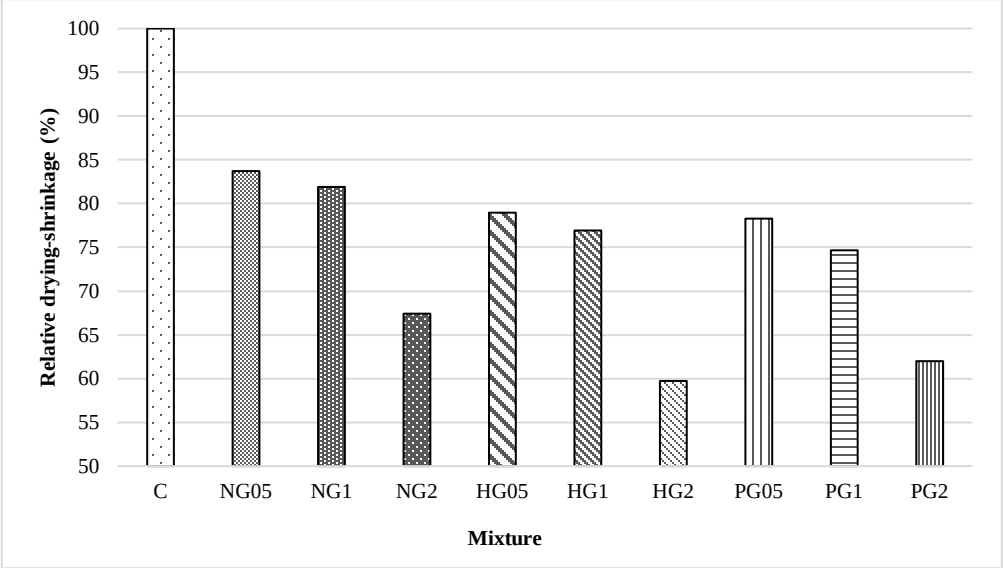

Figure 2. Relative drying-shrinkage rates of mortar mixes

3.3. Compressive Strength

The 7- and 28-day compressive strengths of the mixtures are shown in Table 5. Regardless of the SRA type and utilization rate, 7- and 28-day compressive strengths of the mixtures were lower compared to the control mixture with the utilization of SRA. When the 7-day compressive strength results were examined, the mixtures containing PG, HG, and NG were decreased by approximately 7%, 12%, and 14%, respectively, compared to the control mixture. In the 28-day compressive strength results, PG, HG, and NG exhibited 5%, 11% and 4% lower compressive strength performance compared to the control mixture. As can be seen from the results, the negative effect on the compressive strength of SRA decreased with the increase of curing time. There were also studies in the literature in which SRA negatively affects the early age compressive strength performance in cementitious systems [14]. In the mentioned studies, it was stated that the negative effect of SRA on the early age compressive strength was due to the prolongation of the setting time by decreasing the alkalinity of the pore solution. Within the scope of the study, it was thought that the negative effect of the utilization of SRA on the 7-day compressive strength performance is due to the delay in setting time as stated in the literature.

Table 5. Compressive strength results of mixtures

Mixtures	Compressive Strength (MPa)		Relative Compressive Strength (%)	
	7-d	28-d	7-d	28-d
C	87.3	97.7	100.0	100.0
NG05	78.2	93.7	89.6	95.9
NG1	77.6	96.3	88.9	98.6
NG2	72.1	90.8	82.6	92.9
HG05	82.4	87.4	94.4	89.5
HG1	76.8	86.4	88.0	88.5
HG2	72.5	89.1	83.0	91.2
PG05	86.1	94.6	98.6	96.8
PG1	82.3	90.8	94.3	92.9
PG2	76.6	94.4	87.7	96.7

4. CONCLUSION

In the study, the effect of using different types and ratios of SRA on the slump-flow performance, drying-shrinkage behavior and compressive strength of cementitious mixtures were investigated. The results are given below:

- Regardless of the SRA type and utilization rate, the PCE requirement and drying-shrinkage behavior for the target slump value were positively affected, while the 7 and 28-day compressive strength was negatively affected by the SRA utilization.
- Slump-flow performance and drying-shrinkage behavior of the mixtures were positively affected by the increase in the SRA utilization rate.
- The negative effect of SRA on compressive strength decreased with the increase of curing time.
- HG and PG admixtures showed similar performance in terms of drying-shrinkage behavior, while NG admixture showed the lowest performance in terms of drying-shrinkage behavior.

ACKNOWLEDGMENT

The authors thank Polisan Kimya A.S for their support in the supply of cement, aggregate and SRA admixtures.

REFERENCES

[1] Zhan, P. M., & He, Z. H. (2019). Application of shrinkage reducing admixture in concrete: A review. *Construction and Building Materials*, *201*, 676-690.

[2] Wu, H., Duan, H., Zheng, L., Wang, J., Niu, Y., & Zhang, G. (2016). Demolition waste generation and recycling potentials in a rapidly developing flagship megacity of South China: Prospective scenarios and implications. *Construction and Building Materials*, *113*, 1007-1016.

[3] Wu, L., Farzadnia, N., Shi, C., Zhang, Z., & Wang, H. (2017). Autogenous shrinkage of high performance concrete: A review. *Construction and Building Materials*, *149*, 62-75.

[4] Mora-Ruacho, J., Gettu, R., & Aguado, A. (2009). Influence of shrinkage-reducing admixtures on the reduction of plastic shrinkage cracking in concrete. *Cement and Concrete Research*, *39*(3), 141-146.

[5] Zhang, W., Hama, Y., & Na, S. H. (2015). Drying shrinkage and microstructure characteristics of mortar incorporating ground granulated blast furnace slag and shrinkage reducing admixture. *Construction and building materials*, *93*, 267-277.

[6] Folliard, K. J., & Berke, N. S. (1997). Properties of high-performance concrete containing shrinkage-reducing admixture. *Cement and Concrete Research*, *27*(9), 1357-1364.

[7] Deboodt, T., Fu, T., & Ideker, J. H. (2015). Durability assessment of high-performance concrete with SRAs and FLWAs. *Cement and Concrete Composites*, *57*, 94-101.

[8] Rajabipour, F., Sant, G., & Weiss, J. (2008). Interactions between shrinkage reducing admixtures (SRA) and cement paste's pore solution. *Cement and Concrete Research*, *38*(5), 606-615.

[9] Saliba, J., Rozière, E., Grondin, F., & Loukili, A. (2011). Influence of shrinkage-reducing admixtures on plastic and long-term shrinkage. *Cement and Concrete Composites*, *33*(2), 209-217.

[10] Tran, N. P., Gunasekara, C., Law, D. W., Houshyar, S., Setunge, S., & Cwirzen, A. (2021). A critical review on drying shrinkage mitigation strategies in cement-based materials. *Journal of Building Engineering*, *38*, 102210.

[11] Yoo, D. Y., Ryu, G. S., Yuan, T., & Koh, K. T. (2017). Mitigating shrinkage cracking in posttensioning grout using shrinkage-reducing admixture. *Cement and Concrete Composites*, *81*, 97-108.

[12] Kioumarsi, M., Azarhomayun, F., Haji, M., & Shekarchi, M. (2020). Effect of shrinkage reducing admixture on drying shrinkage of concrete with different w/c ratios. *Materials*, *13*(24), 5721.

[13] Gao, S., Wang, Z., Wang, W., & Qiu, H. (2018). Effect of shrinkage-reducing admixture and expansive agent on mechanical properties and drying shrinkage of Engineered Cementitious Composite (ECC). *Construction and Building Materials*, *179*, 172-185.

[14] Mehdipour, I., & Khayat, K. H. (2018). Enhancing the performance of calcium sulfoaluminate blended cements with shrinkage reducing admixture or lightweight sand. *Cement and Concrete Composites*, *87*, 29-43.

[15] Mardani-Aghabaglou, A., Altun, M. G., Ozen, S., & Ramyar, K. (2017). Effect of shrinkage reducing admixture on drying shrinkage of mortars and its compatibility with water reducing admixture. *Concrete Congress, Turkey*.

[16] Gettu, R., & Roncero, J. (2002). Long-term behoviour of concrete incorporoting o. *Indian Concrete Journal*, 76 (9), 586–592

[17] Yoo, D. Y., Kang, S. T., Lee, J. H., & Yoon, Y. S. (2013). Effect of shrinkage reducing admixture on tensile and flexural behaviors of UHPFRC considering fiber distribution characteristics. *Cement and Concrete Research*, *54*, 180-190.

[18] Collepardi, M., Borsoi, A., Collepardi, S., Olagot, J. J. O., & Troli, R. (2005). Effects of shrinkage reducing admixture in shrinkage compensating concrete under non-wet curing conditions. *Cement and Concrete Composites*, *27*(6), 704-708.

Adaptive neuro-fuzzy inference system models based on particle swarm optimization and genetic algorithms for bidirectional deep drawing

Amir Nemati[1]*. Dennis Bäcker[1] . Peter Muller[2] . Welf-Guntram Drossel[1,2]

Abstract

The adaptive neuro-fuzzy inference system modeling is an efficient tool for uncertain relationships and input parameters in multidimensional process problems. We applied this approach to the bidirectional deep drawing process in this work. Bidirectional deep drawing on servo screw presses is a manufacturing process for sheet metal forming. This process with freely programmable force and motion functions lead to innovative forming technologies for the deep drawing of sheet metals. The deep drawing process is usually complex and nonlinear dynamics. Therefore determining ideal process parameters for deep drawing processes to control failures requires a broad understanding of the process and a challenge for the modeling as the basis of optimized process control. For instance, a Genetic Algorithm (GA) and a Particle Swarm Optimization (PSO) algorithm are used in an Adaptive Neuro-Fuzzy Inference System model to predict thickness and crack that may occur near the bottom of the part due to extreme thinning. Moreover, a database composed of 160 values was obtained using the finite element method (FEM) calculations for training and validating the ANFIS model with the different optimization approaches. This research has shown that the mean error (ME) for the ANFIS model after optimization with the PSO algorithm is 0.007, whereas ME after optimization with the GA algorithm is 0.017.

Keywords: ANFIS, Heuristic algorithms, Bidirectional Deep Drawing

1. INTRODUCTION

Deep drawing is a sheet metal forming process to manufacture complicated 3-D parts from thin sheet metals. In many industries, Deep Drawing is an essential metal forming process. Deep drawing is the most challenging in manufacturing to a faultless result. Indeed, with a deep drawing of sheet metal parts, the local weak point is mainly located at the outlet of the radius. In the local weak, the stress from the processing load is at its highest level; therefore, hardening is at its lowest in weak points. In the process, the sidewall indirectly transfers the drawing force from the flange to the bottom of the part and occurs sheet metal thinner; then, the bottom crack will occur at the weak point due to excessive thinning [1–2].

To solve this problem, Bidirectional deep drawing is suggested (Fig. 1). Bidirectional deep drawing is the approach that can increase work hardening at the local weak point by bending back and forth without damaging the deep-drawn part. In bidirectional deep drawing, the best possible process result or output to be ensured is the value of thickness in a critical position. Indeed, the quality values depend on influencing variables [3–5].

[1] *Corresponding author: Chemnitz University of Technology, Faculty of Mechanical Engineering, Institute for Machine Tools and Production Process, Reichenhainer Str. 70, 09126, Chemnitz, Saxony, Germany. amir.nemati@mb.tu-chemnitz.de*

[2] *Fraunhofer Institute for Machine Tools and Forming Technology, IWU, Nothnitzer Straße 44, 01187, Dresden, Saxony, Germany*

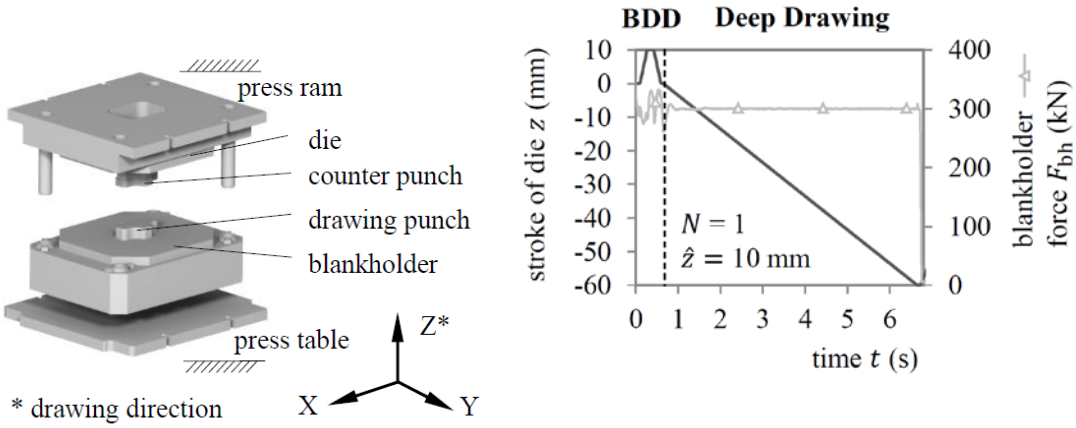

Figure 1. (a) Tool step for bidirectional deep drawing [5] *(b) Process functions for bidirectional deep drawing [5]*

2. PROBLEM STATEMENT

Various types of models are used to describe these relationships for an optimal process flow between input and output parameters and to reduce the error and predict the amount of sheet thickness in a critical position. One approach is physical and theoretical modeling. However, this approach is unsuitable for bidirectional deep drawing optimal process flow because bidirectional deep drawing is a system with a nonlinear behavior and complexity, and conventional physical modeling and theoretical modeling, due to the low information and lack of precise knowledge about the system, is an imprecise model. Therefore, in the bidirectional deep drawing process, many of the phenomena are highly complex and interact with many factors that high process performance cannot be achieved with mathematical relationships because we have to simplify the model, which forces us to accept a certain amount of imprecision and uncertainty in mathematical models that cannot achieve acceptable results for the dynamic behavior of the systems.

In such situations, a data-driven black-box nonlinear system provides a reasonable approximation of nonlinear systems. These approaches create models based on measured or simulated input and output data of the process and require little, no physical, or formal information. Indeed, it has been observed that black-box models such as neural networks (ANN) and fuzzy-logic-based models are widely used to build models of the manufacturing process from measured or simulated input-output data. These approaches perform better than statistical models and mathematical equations. However, artificial neural networks and fuzzy logic have limitations. The main difficulty of neural network models can work with numerical information or data-driven and big data. Consequently, the neural network cannot model from a knowledge base data from human respective engineering knowledge, and the neural network has the main challenge with small data. In fuzzy logic, difficulties are constructing the membership function's shape and fuzzy rules, which are determined using trial and error by the operator. The problem is essential when fuzzy logic is applied to a complex system [6].

The Adaptive Neural Network Fuzzy Inference System (ANFIS) is suggested to solve the challenges. The ANFIS combines the advantages of both artificial neural networks and fuzzy inference systems. The ANFIS has some advantages, including capturing the nonlinear structure of a process, adaptation capability, and rapid learning capacity. The main challenge in the training phase for the ANFIS model is the optimization approach. Because the problem is that globally optimal solutions can not be found in some class problems, Metaheuristic Optimization such as Genetic Algorithm (GA) and Particle Swarm Optimization (PSO) is suggested [7].

3. METHODOLOGY

3.1. Adaptive Neuro-Fuzzy Inference System

Combining the ANN and fuzzy-set theory can provide advantages and overcome the disadvantages of both techniques. The ANFIS model can be trained without expert knowledge sufficient for a fuzzy logic model. The ANFIS model has the advantage of having both numerical and linguistic knowledge. ANFIS also uses the ANN's ability to classify data and identify patterns. Compared to the ANN, the ANFIS model is more transparent to the user and causes fewer memorization errors. The most commonly used fuzzy inference systems are Mamdani and Sugeno. The main difference between Mamdani and Sugeno is that the output membership functions of the Sugeno system are either linear or constant [8]. In this study, the Sugeno-type fuzzy inference system was used because the Sugeno-type system is more computationally efficient than the Mamdani type.

As seen in Fig. 2, the structure of ANFIS consists of five layers, which respectively are called, the fuzzification layer, rule layer, normalization layer, defuzzification layer, and summation layer [7]. In ANFIS, successful training is essential because led to obtaining sufficient results. The training phase in ANFIS means the determination of the parameters and uses the existing input-output data pairs during training belonging to these parts using an optimization algorithm.

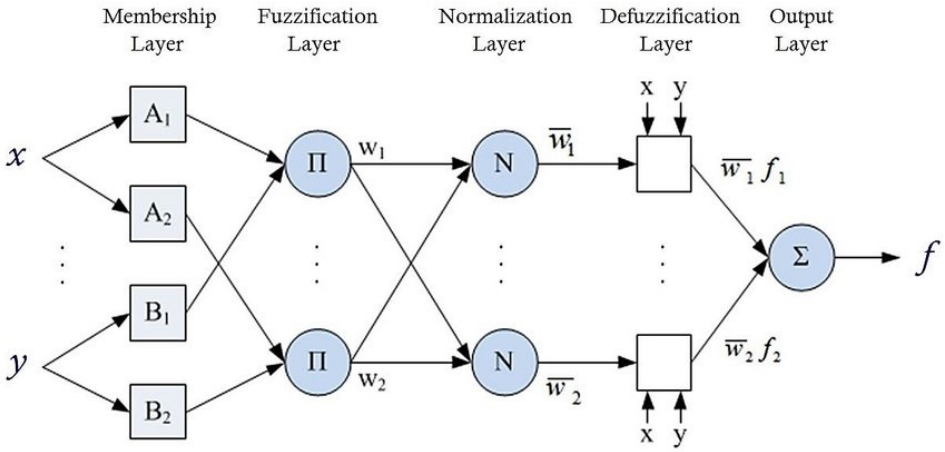

Figure 2. Structure of ANFIS model [7]

3.2. Fuzzy c-means Clustering

Fuzzy clustering, respectively fuzzy c-mean (FCM), is one of the robust unsupervised methods for analyzing data and building models. In many cases, fuzzy clustering is softer, and the boundaries between several classes are not sharp. For example, it means the Objects on the boundaries between several classes do not fully belong to one of the classes but are assigned membership degrees between 0 and 1, indicating their partial membership. It means the FCM gives the flexibility to represent that data points can belong to more than one cluster. The fuzzy c-means algorithm is numerous widely used [9].

3.3. Metaheuristics Optimization Algorithms

Metaheuristics are a family of algorithmic techniques helpful in solving complex problems. Metaheuristics algorithms are appealing optimization strategies for solving nonlinear programming problems characterized by non-convex, disjoint and noisy objective functions. This fact determines them from exact techniques, which do come with verification that the optimal solution will be found in a limited amount of time. Metaheuristics are therefore explicitly developed to find a "good sufficiently" solution in a computing time that is "small sufficiently." Metaheuristics algorithms can make intelligent optimization schemes that combine elements such as stochasticity, adaptation, and learning. It means that the Metaheuristics algorithms can adapt to their environment through evolution if it changes the information from the search steps [10].

3.2.1. Genetic Algorithms

A Genetic Algorithm (GA) is a member of a general class of optimization algorithms known as Evolutionary Algorithms (EA), which simulate a fictional environment based on the theory of evolution to deal with various mathematical problems, especially those related to optimization. Also, Genetic Algorithms can be categorized as a subset of Metaheuristics, which are general-purpose tools and algorithms to solve optimization and unsupervised learning problems.

GA activates according to the principle of survival of the fitness on a population of potential solutions to create better approximate options towards a solution. At each solution generation, new approximations set is produced by selecting individuals based on the fitness level in the problem domain. This practice leads to the growth of well-suited populations. For example, a gene sequence represents a candidate solution in the GA technique called a chromosome. The chromosome potential is named its fitness function, which is assessed through objective function.

Population means a set of selected chromosomes subjected to the number of iterations (generations). For each generation, a new population is created by the operators of GA, such as selection, crossover, and mutation. Exceptionally fit individuals are given chances to replicate by exchanging their genetic statistics. This creates a new offspring solution that would share the good characteristics of parents. Mutation operation is employed crossover subsequently by shifting specific genes in the strings. The offspring can replace a smaller number of fitness individuals or the whole population. This assessment and selection of reproduction sequence are continuously performed until an acceptable solution is obtained. Therefore, The GA process will then operate according to the five steps: Initialization, Selection, Reproduction, Evaluation, and Termination [11, 12].

3.2.1. Particle Swarm Optimization

One population-based optimization algorithm that is inspired by the motion of birds and fish is Particle swarm optimization (PSO).

PSO is initialized with a population, which are of random solutions, and the search for the optimal solution is performed by updating particle positions. The PSO algorithm should create a population of particles that has been initialized at a random position and a velocity. Positions and velocities are adapted, and the function is evaluated with the new coordinates at each time step. Therefore, the coordinates in a vector are stored if a particle located a pattern that is better than any it has discovered previously. The difference between an individual's current position and the best point found is added in this situation.

Additionally, each particle is defined within the context of a topological neighborhood, including itself and some other particles in the population. Other parameter that should be added to its velocity for the next time step is the weighted difference between the individual's current position and the neighborhood's best position. Therefore, These adjustments allow the particle to move around the space and cause it to search around the two best positions [13–15].

4. DATA COLLECTION AND DATABASE

One database is available in origin to evaluate the process data of the bidirectional deep drawing. The comprehensive database is numerically calculated in respectively simulation database. The database from simulation results is contained 160 samples. Our simulation data, with 6 inputs and 1 output Table 1.

In this work, the modeling with multi-input single-output (MISO) systems because the aim is to analyze the influence of the inputs of output. The FCM clustering has been defined as 10 classes. It means with minimal error in this algorithm, the data in 10 classes are separated to train the model. We had separated the simulation data into 70 percent for training and 30 percent for test data.

Table 2. Setup the parameters for computer simulation (FEM) of the bidirectional deep drawing process [5]

	Parameters		Reference Value	Range	Unit
Influence Parameters	Amplitude	$\hat{Z}$	10	0 … 10	mm
	Cycles	N	1	1; 2 … 10	
	Initial Motion	Δz	0	-10 … 10	mm
	Blankholder Force	F	300	50 … 500	kN
	Friction Coefficient	μ	0.05	0.05 … 0.15	
	Scale Factor of Flow Curve	S	1.0	0.8 … 1.2	
Result	Sheet Tickness	s			mm

5. RESULTS AND DISCUSSION

In this work, the nonlinear multi-input single-output (MISO) has been expressed that has been modeled with ANFIS. Therefore, the ANFIS model should have a minimal error with a nonlinear system. Therefore, the parameters for the membership function should be estimated. The approaches to solving this problem are the GA and PSO algorithms. Since both approaches are data-based, a basis for a comparative discussion of the results of the modeling approaches is given based on the percentage mean error (ME) and mean square error (MSE) for the approaches.

After modeling and optimization with a genetic algorithm, The amount of training (Fig. 3) and test data (Fig 4) were evaluated separately. As shown in both figures, the ANFIS model could estimate the sheet's thickness very accurately. At the same time, this model can significantly detect and predict the least amount of thickness at the critical point. The mean value of difference and standard deviation of original output and the amount of prediction for training and test data were calculated separately. The amount of standard deviation in the training data is 0.085293 and in test data is 0.09232. Therefore, the amount of standard deviation in the test data is greater than in the Train data.

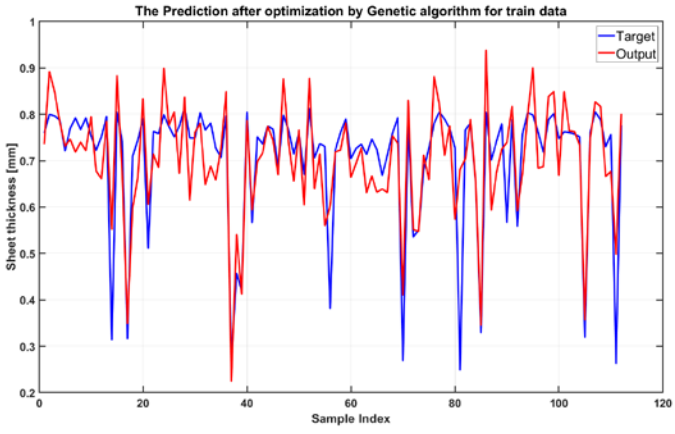

Figure 3. Comparison of the predictions output and target output after optimization by GA for train data

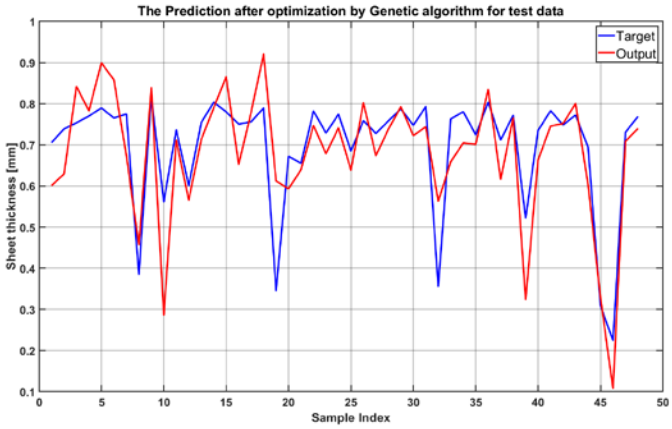

Figure 4. Comparison of the predictions output and target output after optimization by GA for test data

After modeling and optimization with a PSO, The amount of training and test data were again evaluated separately. As shown in Fig. 5 and in Fig. 6 ANFIS model with PSO optimization algorithm was able to estimate the thickness of the sheet very accurately as GA algorithms. At the same time, this model has a significant ability to detect and predict the least amount of thickness at the critical point. Also, the mean value of difference and standard deviation of original output and the amount of prediction for training and test data were calculated separately. The amount of standard deviation in the training data is 0.053468 and in test data is 0.092984. Therefore, the amount of standard deviation in the test data is greater than in the Train data. Interestingly, the error value in the PSO optimization algorithm is much less, and the error values are more focused on the mean point.

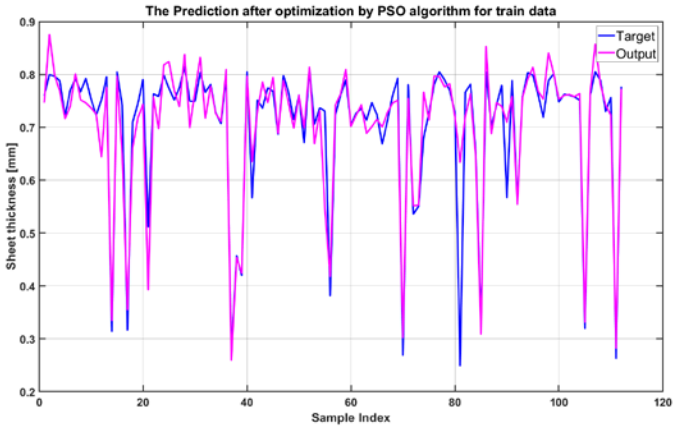

Figure 4. Comparison of the predictions output and target output after optimization by PSO for train data

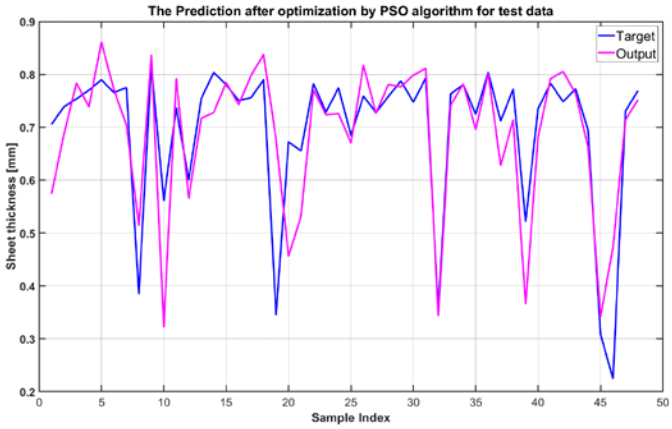

Figure 6. Comparison of the predictions output and target output after optimization by PSO for test data

In this Fig. 7, the amount of mean error and mean square error in the two optimization algorithms are compared. The ME error has the meaning of an average of the nonlinear (here 6-dimensional) modeled map from the real map, averaged over all grid points, and the mean square error is the average of the squares of the errors from the prediction value from the model. This diagram has shown that the mean error (ME) for the ANFIS model after optimization with the PSO algorithm is 0.007, whereas ME after optimization with the GA algorithm is 0.017. This figure has shown that the MSE for the ANFIS model after optimization with the PSO algorithm is 0.00852, whereas MSE after optimization with the GA algorithm is 0.00865. It should be noted here that the amount of training data was very small, and in fact, we were dealing with small data.

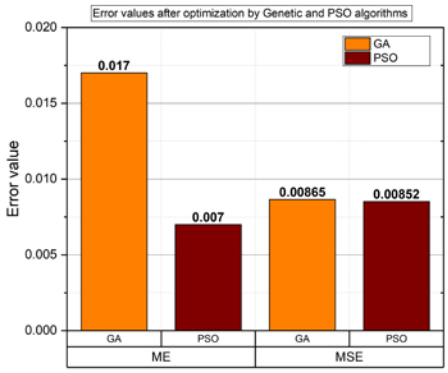

Figure 7. Comparison of GA vs. PSO optimization algorithms ME and MAE error for the output

6. SUMMARY

The bidirectional deep drawing process was introduced as an efficient method. The motivation and purpose were to predict the amount of sheet thickness at critical points with the help of computational intelligence. The model used, The ANFIS model, combines the advantages of both artificial neural networks and fuzzy inference systems. The evolutionary algorithms for optimizing ANFIS modeling are used. We selected ten classes to Train the ANFIS model, in which the data were classified using the Fuzzy C Mean algorithm.

After evaluating the results, it was found that the amount of Mean error is higher than the MSE value for the Genetic algorithm and comparatively high for the output. We also show the amount of prediction error in the

algorithm PSO is smaller than the GA algorithm. And in the end, it is worth mentioning that the ANFIS model has been able to provide an acceptable prediction with small amounts of data.

REFERENCES

[1]. Behrens B-A, Brosius A, Hintze W, et al (2021) Production at the leading edge of technology: Proceedings of the 10th Congress of the German Academic Association for Production Technology (WGP), Dresden, 23-24 September 2020. Springer Berlin Heidelberg, Berlin, Heidelberg

[2]. Altan T, Tekkaya AE (2012) Sheet metal forming. ASM International, Materials Park, Oh

[3]. Kriechenbauer S, Muller P, Mauermann R, Drossel W-G (2021) Evolutionary optimization of deep-drawing processes on servo screw presses with freely programmable force and motion functions. Procedia CIRP 104:1482–1487. https://doi.org/10.1016/j.procir.2021.11.250

[4]. Kriechenbauer S, Mauermann R, Muller P (2014) Deep Drawing with Superimposed Low-frequency Vibrations on Servo-screw Presses. Procedia Engineering 81:905–913. https://doi.org/10.1016/j.proeng.2014.10.116

[5]. Kriechenbauer S, Muller P, Mauermann R, Drossel W-G (2021) Extension of Process Limits with Bidirectional Deep Drawing. In: Behrens B-A, Brosius A, Hintze W, et al (eds) Production at the leading edge of technology. Springer Berlin Heidelberg, Berlin, Heidelberg, pp 96–104

[6]. Hametner C, Jakubek S (2013) Local model network identification for online engine modelling. Information Sciences 220:210–225. https://doi.org/10.1016/j.ins.2011.12.034

[7]. Karaboga D, Kaya E (2019) Adaptive network based fuzzy inference system (ANFIS) training approaches: a comprehensive survey. Artif Intell Rev 52:2263–2293. https://doi.org/10.1007/s10462-017-9610-2

[8]. Takagi T, Sugeno M (1985) Fuzzy identification of systems and its applications to modeling and control. IEEE Transactions on Systems, Man, and Cybernetics SMC-15:116–132. https://doi.org/10.1109/TSMC.1985.6313399

[9]. de Oliveira JV, Pedrycz W Advances in Fuzzy Clustering and Its Applications. 457

[10]. Dréo J (2006) Metaheuristics for hard optimization: methods and case studies. Springer, Berlin

[11]. Angelov PP, Buswell RA (2003) Automatic generation of fuzzy rule-based models from data by genetic algorithms. Information Sciences 15

[12]. Angelov P, Guthke R (1997) A genetic-algorithm-based approach to optimization of bioprocesses described by fuzzy rules. Bioprocess Engineering 16:299. https://doi.org/10.1007/s004490050326

[13]. Bonyadi MR, Michalewicz Z (2017) Particle Swarm Optimization for Single Objective Continuous Space Problems: A Review. Evolutionary Computation 25:1–54. https://doi.org/10.1162/EVCO_r_00180

[14]. E. J. Solteiro Pires, J. A. Tenreiro Machado, P. B. de Moura Oliveira (2009) Particle Swarm Optimization: Dynamical Analysis through Fractional Calculus. INTECH Open Access Publisher

[15]. E. Alfassio Grimaldi FG (2004) PSO as an effective learning algorithm for neural network applications. In: Proceedings. ICCEA 2004. 2004 3rd International Conference on Computational Electromagnetics and Its Applications, 2004. IEEE, Beijing, China, pp 557–560

ICETI

6TH INTERNATIONAL CONFERENCE ON ENGINEERING TECHNOLOGY AND INNOVATION

Western Michigan University

National University of Public Service

International University of Sarajevo IUS

University of Cincinnati

Turkish Airlines

CNR Group